Vicarious calibration of the Ocean PHILLS hyperspectral sensor using a coastal tree-shadow method

Anthony M. Filippi,[1] Kendall L. Carder,[2] and Curtiss O. Davis[3]

Received 31 May 2006; revised 31 August 2006; accepted 4 October 2006; published 23 November 2006.

[1] Ocean color remote-sensing systems require highly accurate calibration (<0.5%) for accurate retrieval of water properties. This accuracy is typically achieved by vicarious calibration which is done by comparing the atmospherically corrected remote-sensing data to accurate estimates of the water-leaving radiance. Here we present a new method for vicarious calibration of a hyperspectral sensor that exploits shadows cast by trees and cliffs along coastlines. Hyperspectral Ocean PHILLS imagery was acquired over East Sound and adjacent waters around Orcas Island, Washington, USA, in August, 1998, in concert with field data collection. To vicariously calibrate the PHILLS data, a method was developed employing pixel pairs in tree-shaded and adjacent unshadowed waters, which utilizes the sky radiance dominating the shaded pixel as a known calibration target. Transects extracted from East Sound imagery were calibrated and validated with field data (RMSE = 0.00033 sr^{-1}), providing validation of this approach for acquiring calibration-adjustment data from the image itself. **Citation:** Filippi, A. M., K. L. Carder, and C. O. Davis (2006), Vicarious calibration of the Ocean PHILLS hyperspectral sensor using a coastal tree-shadow method, *Geophys. Res. Lett.*, *33*, L22605, doi:10.1029/2006GL027073.

1. Introduction

[2] Imaging spectrometers (i.e., hyperspectral imagers) collect continuous spectra for each pixel in the scene, and the added spectral information is essential for resolving the complexity of coastal environments. To estimate near-surface water properties, accurate sensor calibration and atmospheric correction are especially important for aquatic environments due to the smaller-magnitude signal compared to a typical terrestrial scene. For an ocean scene, approximately 90% of the at-sensor signal can be attributed to atmospheric effects [*Gordon and Clark*, 1981]. Because of this, a 5% sensor calibration error can result in an error of as much as 50% in the water-leaving radiance. Further, since sensor performance can change with time (e.g., due to vibrational and/or thermal changes in instrument performance), periodic vicarious sensor calibration is required [*Reinersman et al.*, 1998]. Various methods have been proposed to calibrate remote sensor data to spectral water-leaving radiance $L_u(\lambda)$ or remote-sensing reflectance $L_u(\lambda)/E_d(\lambda)$ or $R_{rs}(\lambda)$, where E_d is the downwelling irradiance at the sea surface and λ is wavelength. Often, spectral water-leaving radiance is measured in a quasi-homogeneous region, and atmospheric optical properties are determined via simultaneous sensor overpass. Within or top-of-the-atmosphere (TOA) radiance can then be modeled, enabling sensor calibration tuning. However, other methods are needed for high spatial resolution sensors deployed over the optically complex waters of the coastal zone [*Reinersman et al.*, 1998]. *Reinersman et al.* [1998] presented a sensor-calibration technique based on cloud shadows. However, the applicability of the approach is limited to when cloud shadows are present within a scene. Here we demonstrate a method of vicarious sensor calibration that can be conducted in the absence of cloud shadows (i.e., when it is optimal to acquire optical imagery). Shadows cast by trees or landforms along coastlines are exploited in a vicarious sensor-calibration framework. The objective of this investigation was to calibrate the Naval Research Laboratory (NRL) Ocean PHILLS (Portable Hyperspectral Imager for Low Light Spectroscopy, [*Davis et al.*, 2002]) hyperspectral sensor using a cloud shadow-free scene, though the general method is transferable to other imaging spectrometers. The method presented here is general and represents a viable strategy to provide vicarious calibration of any sensor in the field.

2. Methods

2.1. Data Sets

[3] During 03–05 August 1998, the hyperspectral airborne Ocean PHILLS sensor was flown over various locations in the case 2 waters surrounding the San Juan Archipelago, in concert with in situ data collection from several boats, including the University of Washington R/V *Barnes* and R/V *Nugget*. The study site is located in a large fjord, East Sound, Orcas Island (approx. 48° 36.5′ N, 122° 51′ W), WA, USA, and the PHILLS image was acquired 05 August 1998 at 10:34 am local time (17:34 UTC), with a ground-projected instantaneous field-of-view (GIFOV) of 3 m. Total sky cloud cover was estimated at ~3%, and a cloud-free image was acquired. The sea truth data included Spectrix and Analytical Spectral Devices, Inc. (ASD) (FieldSpec Dual UV/VNIR) spectroradiometer above water measurements $L_u(\lambda)$ and derived $R_{rs}(\lambda)$ and HOBI Labs HydroScat-6-derived backscattering b_b [*Maffione and Dana*, 1997]. A SLM-Aminco DW-2C dual-beam spectrophotometer was used to derive the laboratory spectral phytoplankton absorption coefficient $a_\phi(\lambda)$ from water samples collected in situ [*Roesler et al.*, 1989]. Discrete water samples were collected adjacent to the R/V Barnes (48° 36.546′ N, 122° 51.028′ W) at 11:16 am local time

[1]Department of Geography, Texas A&M University, College Station, Texas, USA.
[2]Department of Marine Science, University of South Florida, St. Petersburg, Florida, USA.
[3]College of Oceanic and Atmospheric Sciences, Oregon State University, Corvallis, Oregon, USA.

Copyright 2006 by the American Geophysical Union.
0094-8276/06/2006GL027073

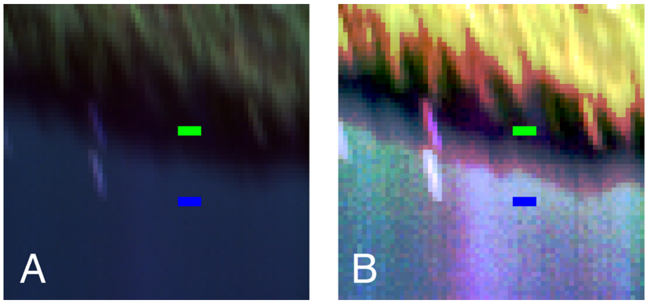

Figure 1. (a) An example pixel pair as shown on a true-color composite Ocean PHILLS image; the upper ROI (ROIs shown as solid rectangles) is in the shaded water area, while the lower ROI is in the direct solar-illuminated water area; (b) same image, but with a Gaussian stretch applied, enabling improved visual contrast between shaded and unshaded water.

(18:16 UTC) at depths of 0, 2, 6, and 16 m, with 510, 535, 265, and 535 mL water filtered for processing, respectively. The Spectrix and ASD spectroradiometers were operated at viewing angle (θ) = 30° and azimuth (ϕ) = 90° relative to the Sun to minimize sun glint.

2.2. Vicarious Calibration

[4] A method for vicarious calibration of the NRL Ocean PHILLS hyperspectral sensor, flown at ~3,050 m altitude, was developed that takes advantage of shadows cast by trees and cliffs along the coast. The PHILLS sensor is currently well-calibrated [*Davis et al.*, 2002], but it was employing a loaner camera and not fully calibrated when the 1998 imagery was acquired for this Puget Sound mission (the usual PHILLS camera had been temporarily substituted with a Pixelvision camera with a slower frame transfer rate). Calibration problems precluded the use of standard atmospheric correction models[e.g., *Gao et al.*, 2000] to correct the remote sensor image data to $R_{rs}(\lambda)$ since calibrated radiance data are required as input. Therefore, a coastal tree-shadow sensor-calibration method was developed that uses pixel pairs in tree-shadowed and adjacent unshadowed waters of similar optical properties; this approach utilizes the sky radiance dominating the shadowed pixels as a known calibration source. East Sound is a typical fjord with high cliffs and a dense forest along the coast. The water is turbid, and the bottom drops off quickly so that the bottom is not visible in the imagery even a few meters from shore. The pixel(s) in the neighboring unshadowed region are assumed to have inherent optical properties (IOPs) identical to the tree-shadowed region due to spatial autocorrelation and the scale of significant optical property variability in the horizontal dimension [*Mobley and Sundman*, 2001]; this neighboring region is illuminated by direct solar photons and skylight. The difference between the total radiance values observed at the sensor for the two regions are utilized in the algorithm, thus allowing the removal of the nearly identical atmospheric radiance contributions to the two signals (i.e., path radiance and Fresnel-reflected skylight). The Ocean PHILLS is a pushbroom imaging spectrometer, and thus, each column of imagery must be calibrated independently. This method is a variant of the method used to calibrate and atmospherically correct video imagery from a blimp by incorporating the blimp shadow from low altitude [*Carder et al.*, 1997] and a simplification of the cloud-shadow method of *Reinersman et al.* [1998].

[5] To demonstrate the method, an algorithm was developed for and applied to an East Sound Ocean PHILLS image (Figure 1). A region of interest (ROI) was delineated on the image in a dark tree-shadow area along the coast that contrasted highly with adjacent solar-illuminated water pixels; a corresponding ROI was delimited in this adjacent illuminated area along the same image column. This pair of ROIs was located on a transect that intersected the position of one of the boats where in situ optical measurements were made. Figure 1 shows an example shaded and solar-illuminated coastal pixel pair. Transects corresponding to the positions of the R/V *Barnes* and the R/V *Nugget* within the PHILLS scene were selected for processing. A heuristic, iterative curve-fitting procedure was employed with atmospherically corrected PHILLS spectra, corrected via RADTRAN, a clear-sky spectral irradiance model [*Gregg and Carder*, 1990], and observed in situ spectroradiometer spectra to derive the calibration equation. RADTRAN is an extension of the *Bird and Riordan* [1986] model to ocean applications with marine aerosols and negligible ground albedo effects assumed for down-welling irradiance. Since atmospheric correction results from exploiting the differences between unshaded and shaded pixels, RADTRAN is used to separate the spectral effects of the direct and diffuse down-welling irradiance fields. The calibration equation for the R/V *Barnes*/Fraser River image transect, whose water properties were influenced by the Fraser River, is as follows:

$$R_{rs} = Raw{*}C - (L_{sky} - 0.015){*}0.085 \tag{1}$$

where Raw = raw data value (Figure 2a); C = calibration factor; L_{sky} = sky radiance (includes Rayleigh and down-welling (↓) aerosol effects); 0.015 = bias (an aerosol radiance and forward-scattering correction); and 0.085 = scaling factor (F). Note that sky reflectance = L_{sky}/E_d and that,

$$C = L_{sky}{*}(F)/S_{shade} \tag{2}$$

and

$$R_{rs}(\lambda) = \frac{L_{neighbor}}{E_d} = \frac{S_{neighbor}}{S_{shade}} {*} \frac{L_{sky}{*}(F)}{E_d}, \tag{3}$$

where L_{sky} is sky radiance; S_{shade} are the (uncalibrated) digital counts for the shaded pixels in the region of interest (ROI); $S_{neighbor}$ are the (uncalibrated) digital counts for the unshadowed, neighboring pixels; $L_{neighbor}$ is the radiance of the direct solar-illuminated, neighboring ROI; E_d is the downwelling irradiance; and $R_{rs}(\lambda)$ is the spectral remote-sensing reflectance (sr^{-1}). The values for C and S are λ-dependent. This approach was validated with field data, thus providing validation of an approach for acquiring calibration-adjustment data from the image itself. The calibration algorithm is summarized in 9 steps as follows:

[6] 1. $L_{shade} = B * L_{sky} + R_{rs} * E_{sky} = cal * S_{shade} = L_{path} + 0.022 * L_{sky} + R_{rs} * E_{sky}$, where L_{shade} is the radiance of the tree-shaded pixels; L_{path} is the path radiance; L_{sky} is derived

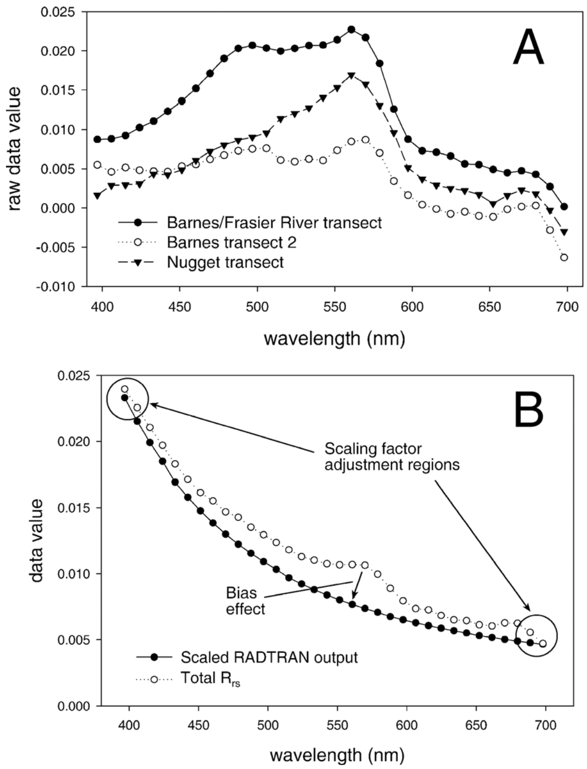

Figure 2. (a) Derived calibration curves prior to scaling for three Ocean PHILLS image transect ROIs, East Sound, WA, 05 August 1998. (b) Calculated total R_{rs} for R/V *Barnes*/Fraser River pixel ROI and scaled modeled RADTRAN sky. Total R_{rs} was derived by first computing a set of calibration factors ((sky irradiance/π)/S_{shade}). This factor was then multiplied by the raw image data values extracted from the ROI near the R/V *Barnes*. This product, with a calibration factor applied, was then divided by the total irradiance computed by RADTRAN. This quotient was multiplied by a scaling factor of 0.25. The scaled RADTRAN sky curve was derived by subtracting a bias of 0.015 from the sky reflectance, calculated as (sky irradiance/total irradiance from RADTRAN). This quantity was multiplied by a constant of 0.34, and the product was multiplied by a scaling factor of 0.25.

from RADTRAN; and 0.022 is the Fresnel reflectance factor for water. B is discussed below.

[7] 2. $L_{sky} \sim$ sky radiance $\sim E_{sky}/B$, where E_{sky} is the RADTRAN-derived sky contribution to downwelling surface irradiance. The constant B corrects for the fact that the path radiance is not for an entire atmosphere, but just up to the aircraft, and it corrects for inaccuracies resulting from a Lambertian sky assumption ($E_{sky} \sim$B * L_{sky}). Since for clear days L_{path} and 0.022 * L_{sky} are the same color, these terms can be combined. L_{path} is mostly Rayleigh scattering; L_{sky} is Rayleigh + aerosol scattering, but aerosol scattering is solar-like and excluded from L_{sky}.

[8] 3. $L_{neighbor} = R_{\mathrm{rs}} * E_d(0) + 0.022 * L_{sky} + L_{path} = R_{\mathrm{rs}} * (E_{sol} + E_{sky}) + \mathrm{B} * L_{sky}$, where E_{sol} is downwelling solar irradiance.

[9] 4. $L_{neighbor} - L_{shade} = R_{\mathrm{rs}} * E_{sol}$

[10] 5. cal * $(S_{neighbor} - S_{shade}) = R_{\mathrm{rs}} * E_{sol}$

[11] 6. cal = $R_{\mathrm{rs}} * E_{sol}/(S_{neighbor} - S_{shade})$

[12] 7. However, R_{rs} is smooth and can be splined to any spectral space. E_{sol} and $S_{neighbor}$ have different spectral spaces and resolutions. Therefore, adjustments must be made as follows:

[13] 8. $S_{neighbor}/S_{shade} = L_{neighbor}/L_{shade} = R_{rs} * E_d/(\mathrm{B} * L_{sky} + R_{\mathrm{rs}} * E_{sky})$.

[14] 9. Solve for B, given a rough estimate of R_{rs} from in situ hand-held spectroradiometer measurements from the R/V FHL *Nugget* or R/V *Barnes*, since all other terms are available using RADTRAN and PHILLS measurements.

[15] This approach does not require knowledge of the spectral resolution of the PHILLS data or consistency of calibration with solar constant resolution or of in situ spectroradiometer resolution. E_d, E_{sky}, and L_{sky} can all be derived from the RADTRAN atmospheric model. R_{rs} is a Spectrix or ASD spectroradiometer ratio, obviating a calibration constant. Calibration (cal) factors all divide out since signals for shade and neighbor pixels are from the PHILLS sensor. Given B and R_{rs} from the R/V *Nugget* or the R/V *Barnes*, for example, cal is derived from step 1 using RADTRAN E_{sky} and E_{sky}/B spectra. Finally, for R_{rs} rather than L_u measurements, solve #8 for R_{rs} (Figure 2b). This methodology ratios out the spectral responsivities for both PHILLS and RADTRAN, so it is permissible that their spectral resolutions be different. Also note that the ratio values of one (e.g., RADTRAN) needs to be splined into the spectral space of the other (e.g., PHILLS).

[16] For this study, atmospheric adjacency effects (e.g., scattering radiance from the forest into the water field-of-view) are considered small at low-contrast visible wavelengths because of 1) the high visibility ($\sim$50 km) and low aerosol content of the atmosphere; 2) the effects of molecular scattering on the adjacency for the shaded and sun-lit pixels are nearly equal because of their spatial proximity [*Reinersman and Carder*, 1995]; and 3) the effects on each are removed by the subtraction process between the adjacent pixels.

3. Results and Discussion

[17] A calibrated PHILLS spectrum for one pixel along the R/V *Barnes*/Fraser River columnar image transect was extracted from the image and compared with spectra acquired in situ (Figures 3a and 3b). Treating a spatially coincident in situ R_{rs} spectrum as a reference standard, the root-mean-squared-error (RMSE) between the two spectra was calculated as 0.00033 sr^{-1} (-1.1944% mean difference) (Figure 3a). A well-calibrated radiance sensor is accurate to about 3% in the laboratory [e.g., *Cattrall et al.*, 2002]. For clear water at 443 nm, typical normalized water-leaving radiance (e.g., $\sim$0.50 mW/cm^2/μm/sr) is >10 times smaller than TOA total radiances ($\sim$6.06 mW/cm^2/μm/sr) [*Gordon et al.*, 1983], boosting that error to 30% for water-leaving radiance for a scene that has perfect removal of atmospheric effects. Without a perfectly accurate sensor, atmospheric correction errors also increase. A calibration that is 5% high in the blue can even yield negative blue water-leaving radiances [*Gordon et al.*, 1983] over bright blue waters. For PHILLS, flying at $\sim$3,050-m altitudes, this 10$\times$ error multiplier reduces to less than 5$\times$ for bright blue water, but more for dark, chlorophyll- and colored dissolved organic matter (CDOM)-rich coastal waters. With-

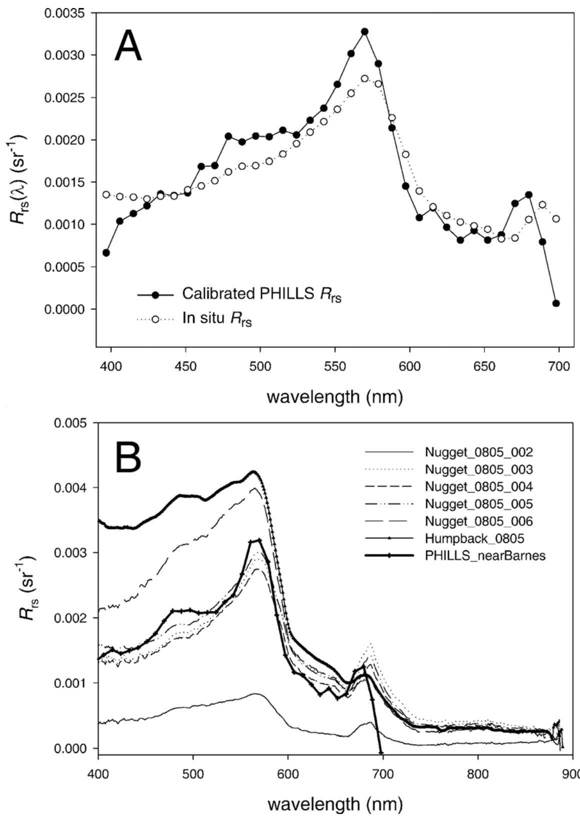

Figure 3. (a) Calibrated PHILLS spectrum for a ROI along the R/V *Barnes*/Fraser River columnar image transect. In situ hand-held spectroradiometer R_{rs} for the same nominal location was convolved to the PHILLS spectral channels to enable RMSE calculation between the two spectra (RMSE = 0.00033 sr^{-1}). (b) Calibrated PHILLS spectrum for an ROI near the R/V *Barnes* (in heavy weight) and in situ spectroradiometer-derived R_{rs} from two boats near the time of sensor overpass. The calibrated PHILLS spectrum is within a reasonable range of variability, as suggested by the field spectra.

out a reasonably well-calibrated sensor, atmospheric correction by standard oceanic techniques [e.g., *Gordon et al.*, 1983] is not possible. Here we derive mean R_{rs} values of $\sim$0.0018 sr^{-1} with $\sim$0.00033 sr^{-1} uncertainty, or about an 18% error in remote-sensing reflectance, and the error at 443 nm was even smaller. These are very reasonable values and quite applicable to estimating pigment absorption values.

[18] The calibrated PHILLS R_{rs} spectrum was additionally evaluated with respect to the accuracy of inversion products derived from it. The Roesler-Perry (R-P) spectral algorithm [*Roesler and Perry*, 1995] was applied to the PHILLS R_{rs} spectrum. The R-P inversion algorithm determines phytoplankton spectral absorption coefficients, total backscattering spectra, and other outputs based on in situ spectral irradiance reflectance or remotely sensed reflectance measurements in absence of spectral variability constraints. The forward component computes irradiance reflectance $\hat{R}(\lambda)$, while the inverse model yields first- and second-order estimates of the spectral phytoplankton absorption coefficient [*Roesler and Perry*, 1995]. $\hat{R}(\lambda)$ closely matches calibrated PHILLS-measured $R_{rs}(\lambda)$ (i.e., $R_{meas}(\lambda)$) (RMSE = 0.00022 sr^{-1}; 1.18 % mean difference) (Figure 4a). Regarding the estimated total spectral backscattering coefficient $b_{bT}(\lambda)$, the Angstrom exponent from the R-P model (-1.50) was similar to that measured in situ by the HydroScat-6 at 440 nm (-1.21). For the second-order estimation of the phytoplankton absorption spectrum, $\mathring{a}_\phi(\lambda)$, the magnitudes of certain portions of the $\mathring{a}_\phi(\lambda)$ curve were inconsistent with the first-order modeled spectral phytoplankton absorption coefficient $\hat{a}_\phi(\lambda)$; however, the salient features and general spectral shape were present in the $\mathring{a}_\phi(\lambda)$ curve (Figure 4b). R-P spectral output at 2-nm resolution was

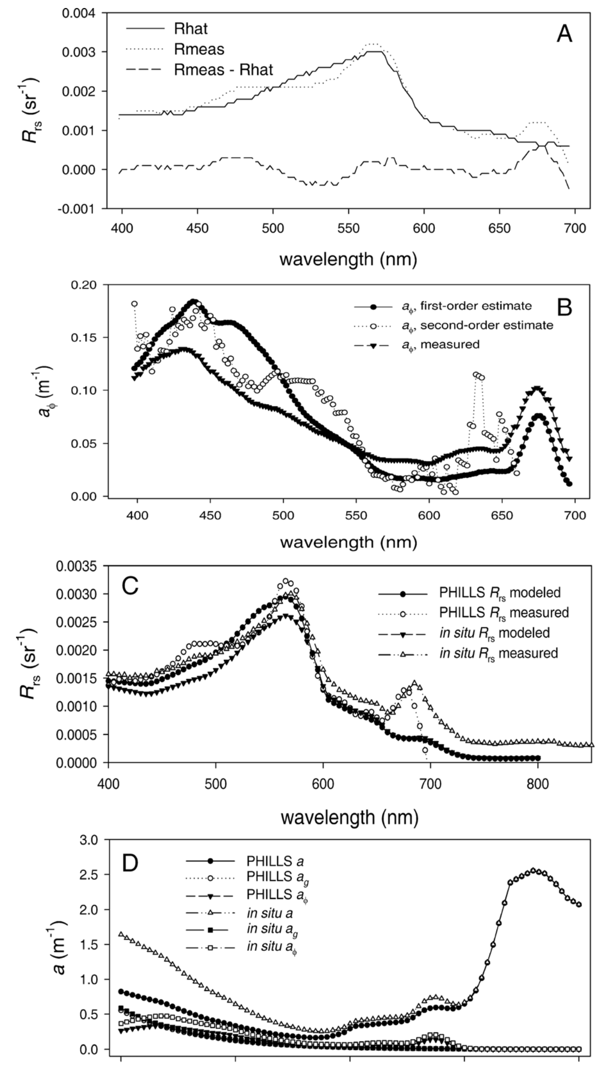

Figure 4. (a) Roesler-Perry (R-P) spectral model-predicted ($\hat{R}(\lambda)$) versus calibrated PHILLS-measured (R_{meas}) reflectance; (b) surface-measured and first- and second-order modeled spectral phytoplankton absorption coefficient ($\hat{a}_\phi(\lambda)$ and $\mathring{a}_\phi(\lambda)$, respectively) estimated from PHILLS R_{rs} inversion using the R-P inversion algorithm; (c) PHILLS- and in situ-measured $R_{rs}(\lambda)$ and the corresponding *Lee et al.* [1999]-predicted $R_{rs}(\lambda)$, respectively; (d) *Lee et al.* [1999]-modeled spectral total absorption (a), gelbstoff absorption (a_g), and phytoplankton absorption (a_ϕ) coefficients derived from PHILLS and in situ spectroradiometer data, respectively. Note that the gelbstoff absorption values at 400 nm ($a_g(400)$) match extremely well.

employed, and spectrophotometer-derived spectra were convolved to the R-P output using a Gaussian filter function from 390 to 750 nm to facilitate RMSE computation. RMSE between R-P first- and second-order phytoplankton absorption estimates and lab spectrophotometer-measured $a_\phi(\lambda)$ from surface water was 0.03040 m^{-1} (−6.5345% mean difference) and 0.24575 m^{-1}, respectively. The $\mathring{a}_\phi(\lambda)$ estimate goes negative in wavelengths longer than 660 nm; thus, assuming only wavelengths up to 660 nm, a RMSE of 0.02805 m^{-1} is obtained (11.331% mean difference). The similarity between the results accrued via calibrated PHILLS data inversion and in situ and laboratory measurements suggests the accuracy of the PHILLS calibration, though some inaccuracies exist with the R-P inversion. Thus, the calibrated PHILLS and field spectra were inverted via the *Lee et al.* [1999] optimization algorithm. Here the comparison was against the derived product using the field spectrum, rather than the measured pigment values so that errors in the algorithm are not levied onto the accuracy/utility of the calibration method. Results are shown in Figures 4c and 4d. The $a_\phi(\lambda)$ spectral shape no longer takes on the errors in the calibration. $a_\phi(443)$ and total absorption at 400 nm ($a(400)$) are within ~45% and 16%, respectively, or vary from their mean values by ±23% and ±8%.

[19] The Ocean PHILLS is a pushbroom imaging spectrometer that uses a two-dimensional array camera with each pixel column representing a different column in the image and each row a different wavelength of the spectrum. The along-track dimension is built-up as the PHILLS flies over the scene. The method presented here provides a vicarious calibration for the columns that intersected the ship measurements. This calibration can be extended to the entire image based upon a flat-fielding approach using a separate scene. During this experiment a relatively homogeneous PHILLS scene acquired over the Strait of Juan de Fuca that does not contain landmass within the image can be utilized to derive a calibration that can be subsequently applied to all of the imagery. Flat-fielding is performed first, followed by calibration. There are several assumptions implicit in applying this correction to the entire scene. Specifically, we assume that CDOM is the dominant absorber at 394 nm, and that L_u at 394 nm is uniform for the small Strait of Juan de Fuca scene. Assuming that the Ocean PHILLS is stable for the duration of this experiment, the calibration can be applied to all of the imagery.

[20] The limitations of the method include: 1) tree-shadows or other shadows along the coastline must be present in the boundary waters in the image; 2) the shadowed and the adjacent direct solar-illuminated pixels must occur in the same image column; 3) the approach is specific to CCD-based push-broom sensors; and 4) water depths should be deeper than about 1.5 optical depths so that gradients in bottom reflectance have a negligible influence. The first and last limitations are typically met for fjords and many rivers, lakes, and estuaries that are eutrophic or turbid.

4. Conclusion

[21] Vicarious calibration of airborne and spaceborne ocean color imagers is necessary to achieve accurate estimates of water properties. An accurate method for vicarious calibration of imaging spectrometers was developed (RMSE = 0.00033 sr^{-1}), which utilizes pixel pairs in tree-shaded and adjacent unshadowed waters, where the sky radiance dominating the tree-shaded pixel is used as a known calibration target. This method is an alternative to a cloud-shadow method developed earlier and is particularly useful for fjords and many rivers, lakes and estuaries imaged under clear-sky conditions.

[22] **Acknowledgments.** This research was supported by an Office of Naval Research (ONR)/NASA Summer Fellowship, Friday Harbor Laboratories, University of Washington, USA. ONR supported the Naval Research Laboratory collection and processing of the PHILLS imagery and in situ data collected on the R/V *Barnes*. Collin Roesler and Mary Jane Perry provided the program code for their model.

References

Bird, R. E., and C. Riordan (1986), Simple solar spectral model for direct and diffuse irradiance on horizontal and tilted planes of the Earth's surface for cloudless atmospheres, *J. Clim. Appl. Meteorol.*, *25*, 87–97.
Carder, M. L., K. L. Carder, and B. L. Weigle (1997), Skylight correction of video images: An airship shadow approach, *Proc. IV International Conference on Remote Sensing for Marine and Coastal Environments*, ERIM Int., Ann Arbor, MI, Vol. II, pp. 631–639.
Cattrall, C., K. L. Carder, K. Thome, and H. Gordon (2002), Solar-reflectance-based calibration of spectral radiometers, *Geophys. Res. Lett.*, *29*(20), 1941, doi:10.1029/2002GL015130.
Davis, C. O., et al. (2002), Ocean PHILLS hyperspectral imager: Design, characterization, and calibration, *Opt. Express*, *10*, 210–221.
Gao, B.-C., M. J. Montes, Z. Ahmad, and C. O. Davis (2000), Atmospheric correction algorithm for hyperspectral remote sensing of ocean from space, *Appl. Opt.*, *39*, 887–896.
Gordon, H. R., and D. K. Clark (1981), Clear water radiances for atmospheric correction of coastal zone color scanner imagery, *Appl. Opt.*, *20*, 4175–4180.
Gordon, H. R., D. K. Clark, J. B. Brown, O. B. Brown, R. H. Evans, and W. W. Broenkow (1983), Phytoplankton pigment concentrations in the Middle Atlantic Bight: Comparison of ship determinations and CZCS estimates, *Appl. Opt.*, *22*, 20–36.
Gregg, W. W., and K. L. Carder (1990), A simple spectral solar irradiance model for cloudless maritime atmospheres, *Limnol. Oceanogr.*, *35*, 1657–1675.
Lee, Z., K. L. Carder, C. D. Mobley, R. G. Steward, and J. S. Patch (1999), Hyperspectral remote sensing for shallow waters: 2. Deriving bottom depths and water properties by optimization, *Appl. Opt.*, *38*, 3831–3843.
Maffione, R. A., and D. R. Dana (1997), Instruments and methods for measuring the backward-scattering coefficient of ocean waters, *Appl. Opt.*, *36*, 6057–6067.
Mobley, C. D., and L. K. Sundman (2001), *Hydrolight 4.2 Users' Guide*, 88 pp., Sequoia Sci., Redmond, Wash.
Reinersman, P., and K. L. Carder (1995), Monte Carlo simulation of the atmospheric point spread function with application to correction for adjacency effect, *Appl. Opt.*, *34*, 4453–4471.
Reinersman, P. N., K. L. Carder, and F.-I. R. Chen (1998), Satellite-sensor calibration verification with the cloud-shadow method, *Appl. Opt.*, *37*, 5541–5549.
Roesler, C. S., and M. J. Perry (1995), In situ phytoplankton absorption, fluorescence emission, and particulate backscattering spectra determined from reflectance, *J. Geophys. Res.*, *100*, 13,279–13,294.
Roesler, C. S., M. J. Perry, and K. L. Carder (1989), Modeling in situ phytoplankton absorption from total absorption spectra in productive inland marine waters, *Limnol. Oceanogr.*, *34*, 1510–1523.

K. L. Carder, Department of Marine Science, University of South Florida, 140 7th Ave S., St. Petersburg, FL 33701, USA.
C. O. Davis, College of Oceanic and Atmospheric Sciences, Oregon State University, 104 COAS Adm. Bldg., Corvallis, OR 97331-5503, USA.
A. M. Filippi, Department of Geography, Texas A&M University, 3147 TAMU, College Station, TX 77843-3147, USA. (filippi@tamu.edu)